Self-Assembly of Colloidal Liquid Crystal in Levitation

Erasmus Mundus Joint Master's Degree: Surface, Electro-, Radiation and Photochemistry (SERP+)

Master Thesis of Jianan QIAN

Supervisors:
Dr. Cyrille HAMON
Chercheur
LPS, Université Paris-Saclay

Dr. Erwan-Nicolas PAINEAU
Chercheur
LPS, Université Paris-Saclay

Table of Contents

Abstract

The common method to build colloidal materials is by the evaporation of a sessile droplet containing nanoparticles. This so-called evaporation induced self-assembly (EISA) process occurring on a substrate, which results in a heterogeneous distribution of nanoparticles on the substrate. To address this problem, an acoustic levitator is implemented to study the self-organization of colloidal liquid crystal in levitated droplets. Three anisotropic one-dimensional colloidal materials (gold nanorods, cellulose nanocrystals, and imogolite nanotubes) were used to study the effect of the morphology and the type of nanoparticles on the final structure of the material. It turned out that the aspect ratio and interactions between nanoparticles play an important role during the self-assembly. Several advantages of self-assembly in levitation were revealed such as its simplicity and robustness to yield colloidal materials with long range ordering. This work open perspectives into the study of EISA in levitating droplet in real time by being coupled with in situ characterization techniques.

Résumé

La méthode commune pour construire des matériaux colloïdaux est l'évaporation d'une gouttelette sessile contenant des nanoparticules. Ce processus d'auto-assemblage induit par évaporation (EISA ; *évaporation induced self-assembly*), qui se produit sur un substrat, entraîne une distribution hétérogène des nanoparticules sur le substrat. Pour résoudre ce problème, un lévitateur acoustique a été mis en œuvre pour étudier l'auto-organisation des cristaux liquides colloïdaux dans des gouttelettes en lévitation. Trois matériaux colloïdaux unidimensionnels anisotropes (nanotiges d'or, nanocristaux de cellulose et nanotubes d'imogolite) ont été utilisés pour étudier l'effet de la morphologie et du type des nanoparticules sur la structure finale du matériau. Il s'est avéré que le rapport d'aspect et les interactions entre les nanoparticules jouaient un rôle important dans l'auto-assemblage. Plusieurs avantages de l'auto-assemblage en lévitation ont été révélés, tels que sa simplicité et sa robustesse pour produire des matériaux colloïdaux avec l'ordre à longue portée. Ce travail ouvre des perspectives dans l'étude de l'EISA dans des gouttelettes en lévitation en temps réel en étant couplé à des techniques de caractérisation in situ.

Acknowledgment

I would like to thank Dr. Cyrille Hamon and Dr. Erwan-Nicolas Paineau, my supervisors, for giving me this precious chance to work in this first-class lab. They imparted professional knowledge, taught me experimental skills, gave me instructions on how to present my ideas, and provided me with many valuable chances.

I also would like to thank other colleagues in Matrix. Dr. Marianne Imperor made suggestions for my presentations. Dr. Claire Goldmann instructed me how to synthesize gold nanoparticles. Dr. Wajdi Chaabani explained theoretical parts to me and helped me with my characterization part. Dr. Jieli Lyu imparted her invaluable experience in experiments to me. Besides, I would like to thank Dr. Claire Boulogne and Dr. Cynthia Gillet at I2BC and Dr. Jeril Degrouard at LPS. They spent time on discussing with me and planned for me to cut the sample.

I am grateful to European Commission for sponsoring my two-year master in Europe. This helped me a lot to improve my adaptability, to learn fast, to respect different cultures and to meet and make new friends from worldwide. Surface, Electro-, Radiation, and Photo-Chemistry (SERP+) family is always in my list. The coordinators of my track: Professor Sandrine Lacombe and Professor Eduardo Marques are nice, and they helped a lot during this master both in study and life. For Eva and Kali, I really bothered them a lot for everything. They helped me a lot patiently and in time with many administration stuffs.

Finally, my parents and my boyfriend, they always respect my choices and cheer me up when I am discouraged.

List of Abbreviations

AA	ascorbic acid
BCC	body-centered cubic
CNC	cellulose nanocrystals
CRE	“coffee-ring effect”
CTAB	hexadecyltrimethylammonium bromide
CTAC	hexadecyltrimethylammonium chloride
EISA	evaporation induced self-assembly
FCC	face-centered cubic
HCP	hexagonal close-packed
INTs	imogolite nanotubes
LC	liquid crystals
LSPR	localized surface plasmon resonance
PMMA	polymethyl methacrylate
NPs	nanoparticles
NRs	nanorods
POM	polarized optical microscopy
SAXS	small-angle X-ray scattering
SEM	scanning electron microscopy
TEM	transmission electron microscopy
TEOG	tetraethoxygermane
UV-vis-NIR	ultraviolet-visible-near infrared

1 Introduction

Inspired by the design principle of nature, scientists are committed to synthesizing complex and organized architectures by nano building blocks. This can be realized by the self-assembly of intricated nanoparticles (NPs), which is a "bottom-up" strategy assembling nanoscale units into larger structures.[1] In the context of mimicking nature, the level of complexity is not yet reached synthetically with colloidal crystal because most NPs are highly symmetric and self-assembly is unconstrained. To overcome these limitations, both NPs shape and the environment should be tuned to "frustrate" crystallization.[2] In these cases, the equilibrium "compromised" arrangement of particles will have inherently low symmetry. Aspects of self-assembly in confinement[3] and shape directed assembly[4, 5] have been studied separately but have seldom been studied together.[6] Herein, this work aims to investigate the effect of the interplay between the shape of NPs defined by different aspect ratio and a tunable confinement on the self-assembly of NPs. As a proof of concept, I focused on shaping a bio-sourced materials (cellulose) into a colloidal material.

1.1 Evaporation Induced Self-Assembly (EISA)

Evaporation induced self-assembly (EISA) is one of the most studied methods to organize the colloidal suspension into an ordered structure or pattern because it is simple and scalable. This approach has been exploited to fabricate various assemblies such as anisometric superlattices by using colloidal particles.[7] It is achieved by depositing colloidal suspensions on a solid support followed by spontaneous evaporation in an open space at room temperature.[8] Normally, drying a nanoparticle solution over a solid substrate produces two-dimensional thin film. Evaporation leads to a progressive increase of concentration to a certain threshold that will eventually induce ordering in the material where different environments force building blocks to reassemble into ordered structures. These structures are kinetically trapped in non-equilibrium states, indicating sensitive dependence on the evaporative route taken. Diverse modes of liquid evaporation affect the types and patterns of deposits. For example, a sessile drop is deposited on a solid substrate and feature a contact angle, contact radius, and drop height, with the wetted region confined by a three-phase (solid, liquid, gas) contact line.[9] After drying, a dense ring-like deposit similar to the coffee stain is observed on the substrate. This ubiquitous phenomenon is called "coffee-ring effect" (CRE) first put forward by Deegan and coworkers.[10] This happens because the contact line remains pinned during the evaporation process and the suspended particles are carried to the drop perimeter due to the radial capillary flow from the center to the edge to replenish the fast loss of solvent. More mechanisms have been further studied to explain this phenomenon, including capillary flow[11] and Marangoni flow[12], three-phase contact line dynamics[13], and particle-particle/particle-interface interaction[14]. All these factors contribute to the nonuniform redistribution of the particles, which will affect the long-range ordering of the final colloidal material.

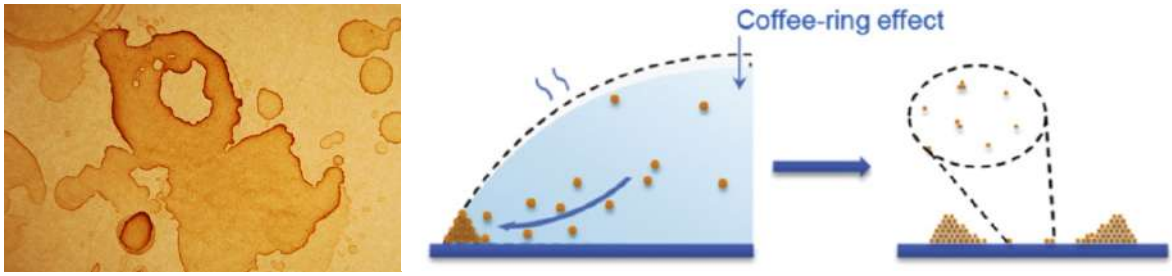

Figure 1.1 "Coffee-ring effect".[15]

A common solution to tackle "coffee-ring effect" is to engineer the properties of droplets while conserving the substrate. For instance, Yang et al. added hydrosoluble polymer additives to SiO_2 microspheres suspensions to avoid coffee ring structure which resulted in the dynamic move of the contact line due to the viscosity and Marangoni effect.[16] However, this approach has several limitations since the resulting thin films are inhomogeneous with non-uniform thickness and suffer from poor cohesion. Another more feasible method is avoiding using the substrate. Li et al. proposed to use a soft template based on microemulsion oil droplets with low boiling point. The nanoparticles self-assembled as the solvent evaporated.[17] The main drawback of this solution is the difficulty of controlling the size or the volume of the resulting droplets. Nevertheless, the idea of using a spherical interface to induce spherical confinement is worth referencing. Another powerful method utilizing this idea is microfluidic method. Cellulose nanocrystals (CNC) were injected into the central channel of a three-channel microfluidic droplet generator. A continuous phase composed of oil and surfactant was injected into other two channels. A spherical confinement was generated, and the droplets were collected in a vial to be equilibrated for several times in cell later.[18]

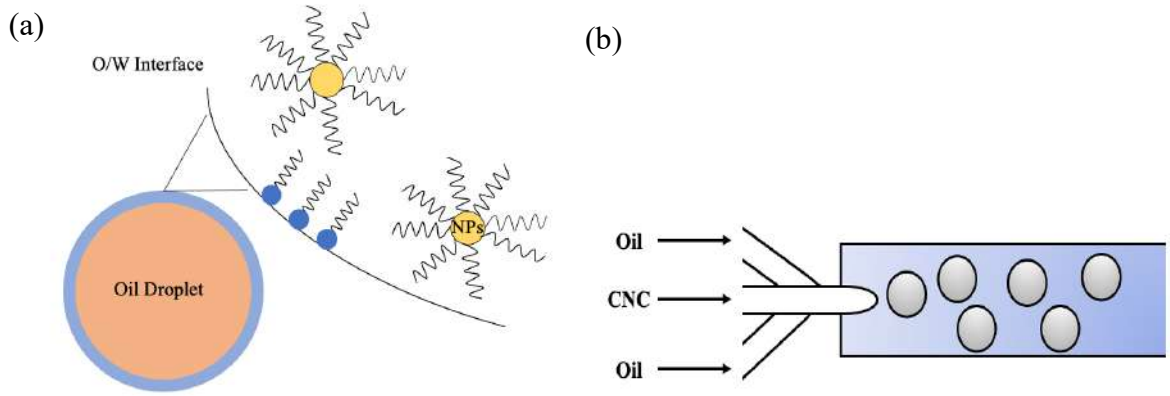

Figure 1.2 Demonstration of self-assembly of nanoparticles using: (a) oil as soft templets; (b) microfluidic method.

However, microfluidic method also faces some challenges: the height of capillaries restricts the dimension of droplets, thus limiting the diameter of droplets to the dimension of the height; such microfluidic system is difficult to handle, many issues should be paid attention to such as obtaining the chip, avoiding leaks, use of syringe pumps, and controlling the flow rate; and finally, the use of surfactants may alter the properties of the nanoparticles and their self-assembly behaviors.

1.2 Acoustic Levitator

In this context, the self-assembly of colloidal particles under acoustic levitation appears as a promising approach. Acoustic levitation is a powerful and versatile tool used in the field of

biology and chemistry, for example, to study the agglomeration of proteins and the assembly of nanoparticles.[19] Since the pioneering work of Bücks and Muller on the levitation of alcohol droplets, different types of acoustic levitation have been proposed including far field acoustic levitation, single beam levitation, and near field levitation. The new generation of levitators uses standing wave levitation, which will be used in this work. In this kind of levitator, small individual piezoelectric transducers are incorporated into the two opposite concave plates treated as sources with a single axis (as shown in Figure 1.3(a)). Compared with traditional Langevin Horn type with a source and a reflector, the two-sources one does not need precise tuning of the parameters such as wavelength. The convenience is given by the transducers acting as small ultrasonic speakers, which create a single field each by adjusting the relative phase between two outputs. Then a collection of these small fields will form a standing wave where particles with the size of around 10 % of the wavelength will be trapped at the nodes as demonstrated in Figure 1.3(b). In this case, tiny polystyrene balls are trapped at the nodes which helps to define the position of the nodes and the wavelength of the standing wave. The single sound wave field and the resulting standing wave can be demonstrated by the simulation in Figure 1.3(c).[20]

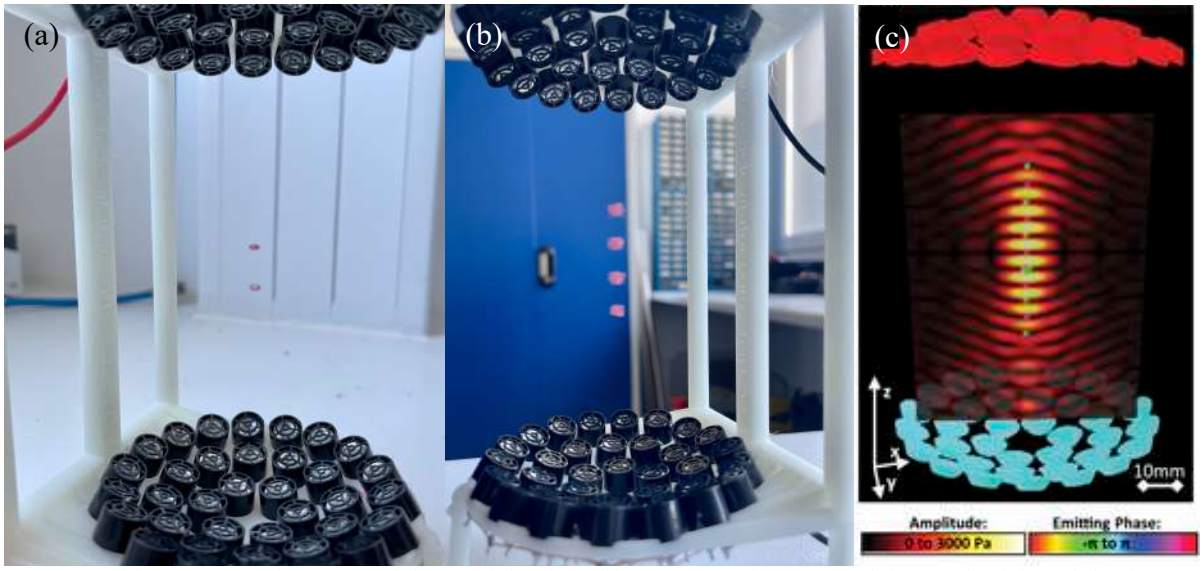

Figure 1.3 (a) An acoustic levitator with levitated droplets; (b) an acoustic levitator with levitated solids and the distances between them are equal; (c) a simulation of the sound wave field.[20]

Compared with the microfluidic approach, acoustic levitation has the following advantages: (1) One can control the volume of the droplet easily; (2) The shape of the droplet can be tuned with the acoustic field, potentially generating a wealth of confining geometries for self-assembly experiments. (3) There is no need of surfactants and a continuous phase to obtain the emulsion.

The acoustic levitator in this work can trap the objects with density around 2.2 g cm^{-3} and 4 mm in diameter when we input 10 W energy. The loading capacity is far beyond what we need in different experiments. The frequency of the transducers is 40 kHz in air. Along with the Arduino Nano, transducers are the signal generators. Also, an amplifier is used to amplify the signal. The backbone is designed and made by 3D-printing technique. Based on the cost of each component, another advantage is of this kind of levitator is economical, typically less than 70€.

1.3 Objectives

In this work, an acoustic levitator based on transducers will be assembled in order to study the self-organization of colloidal liquid crystal in levitated droplets, which gives us insights to the following aspects:

(1) Levitation enables self-assembly without substrate. Both collective properties and individual nanoparticles will be studied. The structure and organization of materials after drying using the acoustic levitator and the substrate will be compared. Advanced characterization tools will be employed to investigate these on nano and micro scales. Three main characterization techniques are initially planned to be used in this work: polarized optical microscopy (POM), electron microscopy, and X-ray scattering.

(2) Rod-like nanoparticles enables researchers to explore the self-assembly of anisotropic particles. In this work, we investigate the self-organization in levitation of 1D "rod-like" NPs that display liquid-crystalline properties. During the progressive evaporation process, phase transitions and macroscopic rearrangements are induced at certain volume fraction. Three materials: cellulose nanocrystals (CNCs), imogolite nanotubes (INTs), and gold nanoparticles (Au NPs) are used to study the effect of aspect ratio on the self-assembly of colloidal suspensions. Aspect ratio for 1D "rod-like" NPs is defined as the ratio of length to diameter. The aspect ratio for Au NPs, CNCs and INTs are around 3, 10, and 100 respectively. Also, three NPs will be mixed to investigate complex hierarchical materials combining individual properties.

1.4 Design of Nanoparticles

1.4.1 Cellulose nanocrystals (CNCs)

Cellulose nanocrystals (CNCs) are highly crystalline materials in the shape of rod with nanometric dimensions (Figure 1.4(a)). This fibrous material is usually derived from wood pulp, bacterial cellulose, tunicin, bast fibers, and linen by hydrolysis of sulfuric acid. CNCs produced by this method are negatively charged due to sulfate half-esters (OSO_3^-) and carboxyl groups (COO^-) grafted on the surface, which will make them colloidally stable in water. In contrast to the uncharged CNCs which tend to gel at relative low concentrations, negatively charged CNCs can be dispersed well in water because of electrostatic double later repulsion between particles.[21]

The liquid crystalline property of CNC suspensions hydrolyzed by sulfuric acid was first reported by Marchessault and his coworkers in 1959. Later, Revol et al. discovered that CNC suspensions self-assembled into a chiral nematic crystalline phase above a certain concentration, which is also known as cholesteric phase. The cholesteric liquid crystal phase is typically consisted of nematic mesogenic molecules with a chiral center which generates intermolecular forces that favor alignment between molecules with a small angle to one another. We can clearly observe the separation of this chiral nematic phase with birefringence and isotropic phase under a polarizer as shown in Figure 1.4(b). The helical self-assembly of CNCs is shown in Figure 1.4(c), one important parameter in this structure is called cholesteric pitch, p, which is defines as the distance between screw threads along the helical axis. This parameter can be defined easily in polarized optical microscopy (POM) and is linked to optical properties.[22]

Due to the helical structure, CNCs possess unique optical properties that can be manipulated depending on the arrangement of the rods. Besides, they are acquired from biomass method which means they are sustainable, renewable, and non-toxic. All these reasons make them a potential candidate as the building blocks to do the assembly.

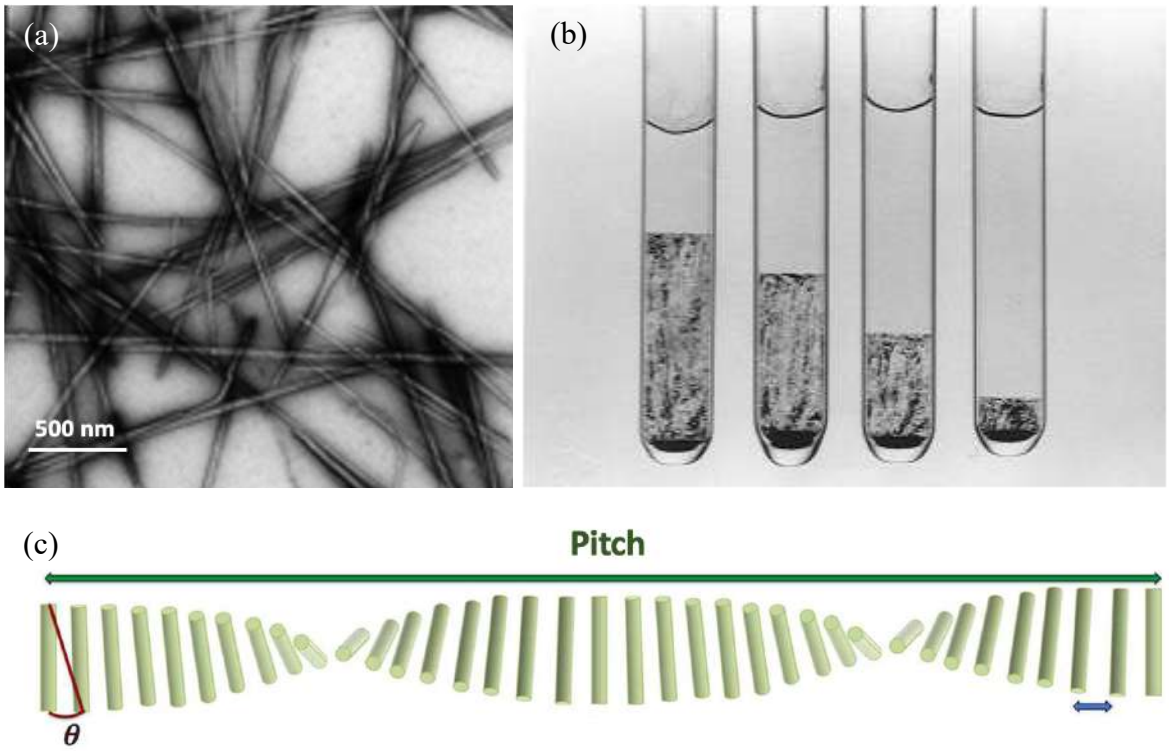

Figure 1.4 (a) Transmission electron microscopy (TEM) image of CNCs; (b) phase separation of CNC suspension: upper isotropic phase and lower chiral nematic phase[21]; (c) scheme of assembled CNCs and pitch.[23]

1.4.2 Imogolite nanotubes (INTs)

Imogolite nanotubes were first discovered naturally in the soils of volcanic origins.[24] They are analogous to the well-known carbon nanotubes in terms of dimensions. However, unlike the latter, they form transparent dispersions, facilitating their optical characterization. The walls of INTs are made of a curved gibbsite-like sheet ($Al(OH)_3$) with the inner hydroxyl surface being substituted by (GeO_3)OH groups. A positive outer wall and a negative inner cavity are acquired by the protonation of different functional groups on different sides.[25,26] Different strategies have been suggested to synthesize these nanotubes. Among them, a straightforward approach has been proposed to synthesize anisotropic double-walled imogolite nanotubes (Ge-DWINTs) using the homogeneous hydrolysis of precursors by thermal decomposition of urea $CO(NH_2)_2$:

$$Ge(OR)_4 + 2AlX_3 + 2CO(NH_2)_2 + 9H_2O \rightarrow (OH)_4Al_2O_3Ge + 4ROH + 2CO_2 + 2H^+ + 4NH_4^+ + 6X^- \quad (1)$$

with R = CH_3, C_2H_5, C_3H_7 and X = Cl, ClO_4, NO_3…

Ge-DWINTs can form stable colloidal dispersions without further exfoliation thanks to the repulsive electrostatic interactions.[27] For sufficient high aspect ratio, colloidal suspensions of Ge-DWINTs display different types of liquid crystal phases,[28] depending on the volume fraction and the initial conditions of the synthesis (Figure 1.5(c)).[26] The liquid crystal phases include nematic and hexagonal columnar phases while at high concentration (volume fraction > 1%), the suspensions turn into birefringent arrested phase.

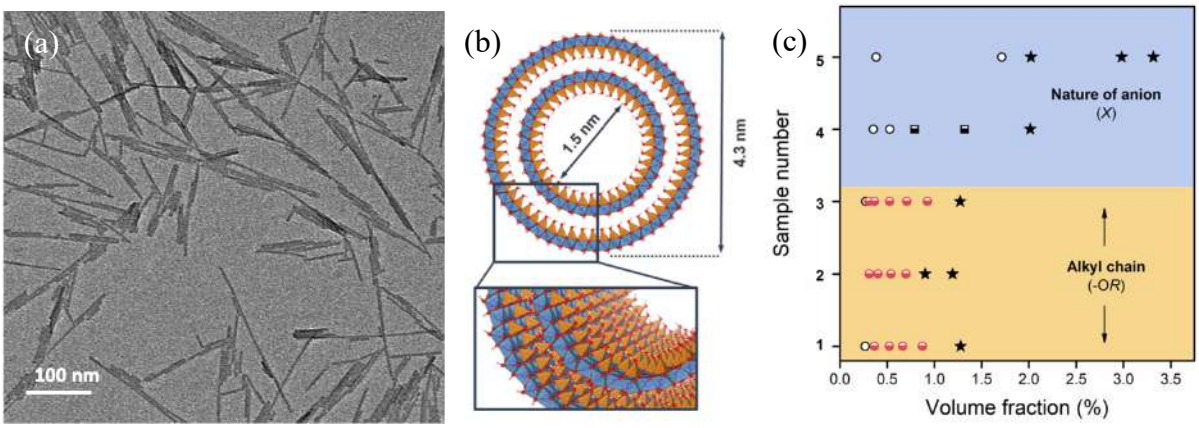

Figure 1.5 (a) TEM image of Ge-DWINTs; (b) structure of Ge-DWINTs; (c) Phase transition as a function of volume fraction for the different Ge-DWINTs. Open circles: isotropic liquid; Half-filled red circles: isotropic-columnar coexistence; Half-filled rectangles: isotropic-nematic coexistence; Stars: arrested phase. Reprinted from Ref. 26.

1.4.3 Gold Nanorods (Au NRs)

Gold Nanoparticles (Au NPs) are promising candidates in various fields such as catalysis, sensors, drug delivery, and therapeutic agents due to their unique properties.[29] Au NPs are well-known for plasmonic properties resulting from the coupling between the electron cloud and electromagnetic radiation whose wavelengths are much larger than the size of AuNPs because of the dielectric-metal interface. This enables them to be applied in sensory applications.[30]

Several approaches can be adopted to synthesize Au NPs such as chemical reduction, electrochemical, and photochemical methods. Among them, chemical reduction method is suitable for the large-scale synthesis and can control the uniformity of Au NPs precisely. This involves mix precursors and some chemical reagents under appropriate conditions which include types of stabilizer and reducing agent and temperature.[31]

In all the methods synthesizing Au NPs in aqueous medium, the seed-mediated growth method is one of the most common and reliable, which can tailor the shape and structure of Au NPs. The seed solution is first produced then different agents are used to adjust various parameters of Au NPs. Different reagents play different roles in the chemical reduction method. Gold and silver precursors are used as sources. Hexadecyltrimethylammonium bromide (CTAB) is used to direct the growth process and to stabilize the Au NPs after synthesis. CTAB and hexadecyltrimethylammonium chloride (CTAC) have a charged ammonium head group which can bind to the surface of the metal. Also, thanks to the hydrophobic effect of the long hydrophobic chains, NPs can stabilize in water. The bromine of CTAB form a complex with Ag which tend to adsorb on the surface of Au and inhibits the growth along axial direction, thus allowing the preferential elongation of Au NRs. Sodium borohydride ($NaBH_4$) and Ascorbic acid (AA) are utilized to reduce Au. AA and silver nitrate are also used as shape-directing reagents.[32] The growth mechanism of this method involves nucleation and growth steps. Simultaneous secondary nucleation and growth can be prevented by separating these two steps.

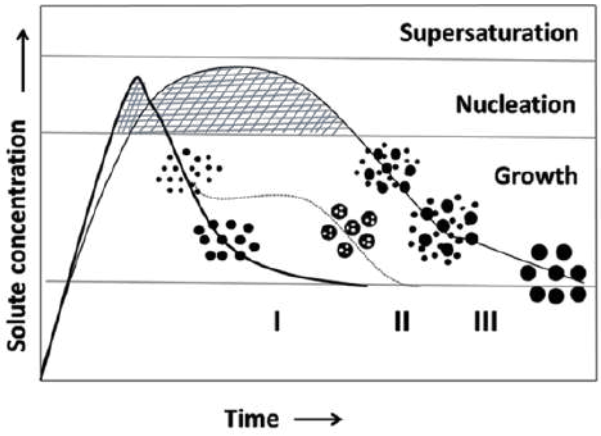

Figure 1.6 Growth mechanisms of uniform Au NPs in solution.[33]

The shape of Au NPs plays an important role in the self-assembled structures, thus affecting collective properties which will determine the applications. In the team of Matrix, LPS, Au NPs with different shapes can be produced, including Au NRs. Seeds are produced by the reduction of Au salts using a strong reducing agent. The seeds with different crystallinity capped by various stabilizing agents will affect the NPs morphology. As shown in Figure 1.7, under different experimental conditions, Au NPs with different shapes are synthesized.

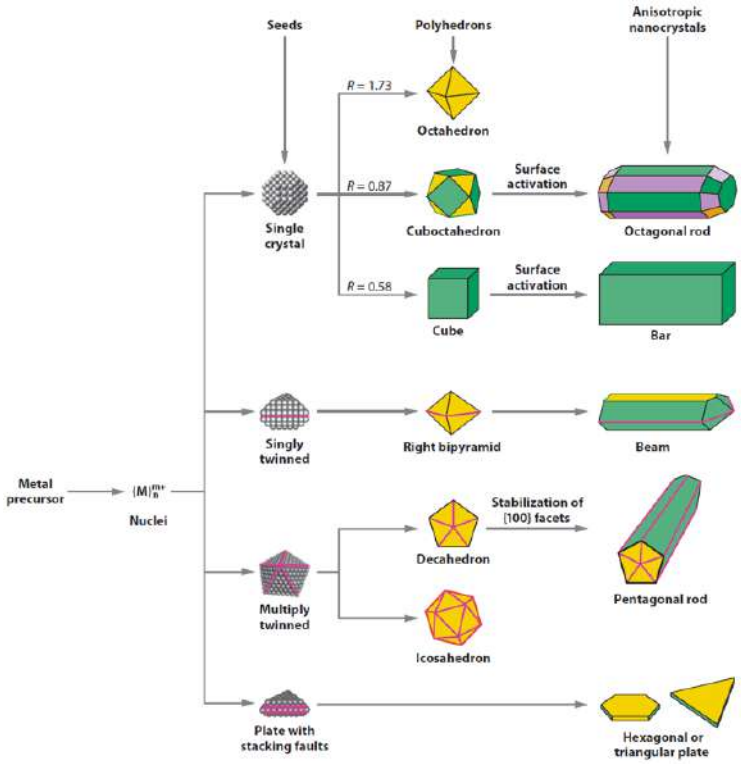

Figure 1.7 Illustration of various shapes obtained from the seeds with different crystallinity.[34]

2 Experimental Section

2.1 Materials

All products were used without further purification. Hexadecyltrimethylammonium bromide (CTAB, ≥99%), hydrogen tetrachloroaurate trihydrate ($HAuCl_4 \cdot 3H_2O$, ≥99.9%), sodium borohydride ($NaBH_4$, 99%), 5-bromosalicylic acid (90%), silver nitrate ($AgNO_3$, ≥99.0%), L-ascorbic acid (AA, ≥99%), hexadecyltrimethylammonium chloride (CTAC, 25 wt % in H_2O), Tetraethoxygermane (TEOG, ≥99.95%), urea ($CO(NH_2)_2$, >99%), NaCl (≥99%), polyethylene glycol (M = 20,000 $g.mol^{-1}$) and ethanol solution (96%) were purchased from Sigma Aldrich. Aluminum perchlorate nonahydrate ($Al(ClO_4)_3 \cdot 9H_2O$, Reagent grade) was purchased from Alfa Aesar. Water purified by reverse osmosis with a resistivity (> 18 MΩ.cm) was used in all experiments. The kit with components of the acoustic levitator was purchased from UpnaLab.

2.2 Preparation of Cellulose Nanocrystals (CNCs)

Cellulose nanocrystals (CNCs) were commercially available and purchased from the U.S. Department of Agriculture (USDA) Forest Products Laboratories (FPL) which were supplied by the University of Maine. CNCs are prepared by sulfuric acid-extracted from wood pulp. The sample was received as a concentrated aqueous dispersion.

2.3 Preparation of Gold Nanorods (Au NRs)

Gold nanorods were synthesized by using the seed-mediated method as indicated in Figure 2.1 The seeds were prepared by injecting 300 μL of freshly prepared 10 mM $NaBH_4$ into the mixture of 4.7 mL of 100 mM CTAB and 50 μL of 25 mM $HAuCl_4$ under vigorous stirring. To avoid the crystallization of CTAB, the whole process remained temperature at 30 °C. In the growth procedure, 450 mg of bromosalicylic acid was dissolved in 250 mL of 100 mL CTAB and 240 mL of purified water under sonication. Then, 476 μL of 100 mM $AgNO_3$ was added to the solution followed by 10 mL of 25 mM $HAuCl_4$. The solution was left stirring at 30 °C for 20 minutes until the absorbance decayed to 0.7 in the UV-vis spectroscopy. Measurements were carried out with Cary 5000 UV-vis-NIR Spectrometer. In *ex-situ* measurements, a baseline used as a reference in all measurements for subtraction was recorded using purified water in a double-beam configuration. Then the growth solution of Au NRs was transferred into the cuvette made of disposable polystyrene (VWR European Cat. NO. 634-0675) with optical path length of 1 cm. After each measurement, the measured solution was poured back to the growth solution in the water bath of 30 °C. The measurements were performed every 30 s until the absorbance decayed to around 0.7. Then 1250 μL of 100 mM ascorbic acid and 800 μL of seeds were injected into the mixture quickly. After 4 h at 30 °C, the mixture was centrifuged 10 min at 10000 rpm at RT and the supernatant was removed. Afterwards, the remaining were collected into one tube. The tube was completed at 40 mL with water and centrifuged 30 – 40 min at 6000 rpm. After the supernatant being removed, the tube was filled with 2.5 mM CTAC to 40 mL and centrifuged at 5000 rpm. The centrifugation was repeated three times to control the concentration of CTAC.

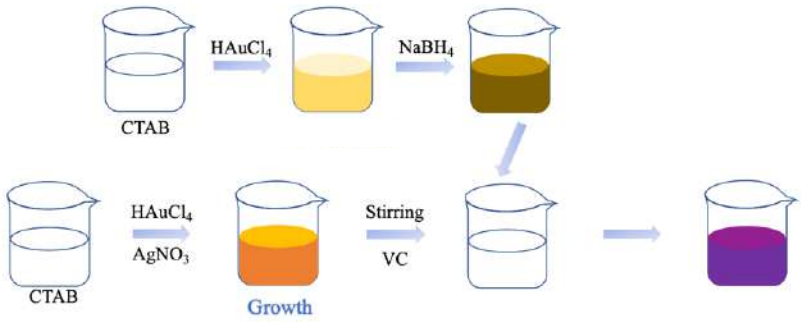

Figure 2.1 Scheme of synthesis of Au NRs.

2.4 Preparation of Double-Walled Aluminogermanate Ge-DWINTs

Ge-DWINTs were synthesized using a single-step method which was first proposed by Amara et al.[28] The detailed procedures are shown in the flowchart (Figure 2.2) Tetraethoxygermane was injected into a solution of aluminum perchlorate nonahydrate and urea (C = 0.2 mol.L^{-1}) under stirring at room temperature. According to Equation. (1), the molar ratio of [Ge]:[Al]:[$CO(NH_2)_2$] equals to 1:2:2. After being stirred for several minutes, the mixture was transferred into a PFTE-lined acid digestion bomb (Zeoclave, Maximator, France). Then, hydrothermal treatment was performed under autogenous pressure at 140 °C for 5 days. The following dialysis using semi-permeable membranes (Spectra/Por®, cut-off = 10 kDa) against ultrapure water was to purify the dispersions. An osmotic stress was then applied to concentrate the imogolite suspension by placing the dialysis membrane in a solution of polyethylene glycol (M_w = 20000 g.mol^{-1}, C = 30 g.L^{-1}) for one week.

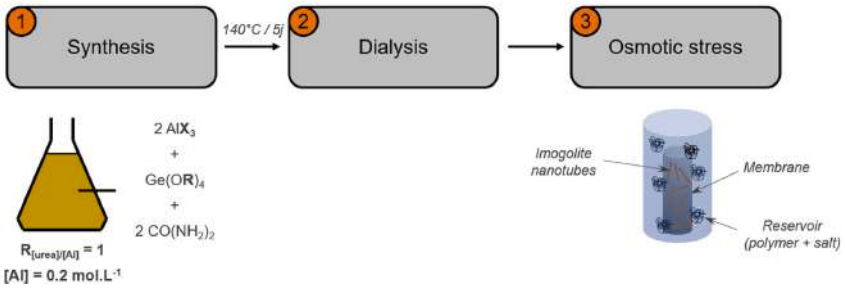

Figure 2.2 Flowchart of synthesis of Ge-DWINTs. Reprinted from Ref. 26.

2.5 Assembly of Acoustic Levitator

All mentioned parts are included in the kit from UpnaLab (Figure 2.3).[20] First, the polarity was marked by using the Arduino. The code provided by UpnaLab was downloaded and installed into the Arduino. One wire was used to connect to A0 gate, another one was connected to GND gate. After the Arduino being connected to the PC, Serial Plotter was selected, and the speed was set to 115200. When the transducer was connected between A0 and GND gate, if the signal declined or remained at 0, the leg connected to GND was marked; If the signal rose to 1023, the leg connected to A0 was marked. After this, transducers were glued to the socket with all the marked legs pointing towards the center of the device. All the legs were wrapped by wires in six concentric rings, and pins were soldered to the wires to stabilizer the connection. Each side of the levitator was connected to one black wire and one red wire. Then the code of levitation was uploaded into the Arduino Nano. The DC supply was connected to the switch. The red wire of the supply was connected to the 12 V input of the driver, and ground was

connected to the middle connector of the driver along with a male-female jumper. Another male-female jumper was inserted into the 5 V input of the driver. These two jumpers were connected to the ground and 5 V gates of the Arduino respectively. 4 female jumpers were used to connect A0, A1, A2, and A3 of the Arduino to IN1, IN2, IN3, and IN4 inputs of the driver respectively. A female-male jumper was inserted into the ground of the Arduino to control the position the samples along the axis of the levitator. To make sure of the synchronized emission of the signals, D10 and D11 were linked. Finally, the driver, shortcuts, transducers, and optimum resonances were tested sequentially to ensure the work of the levitator.

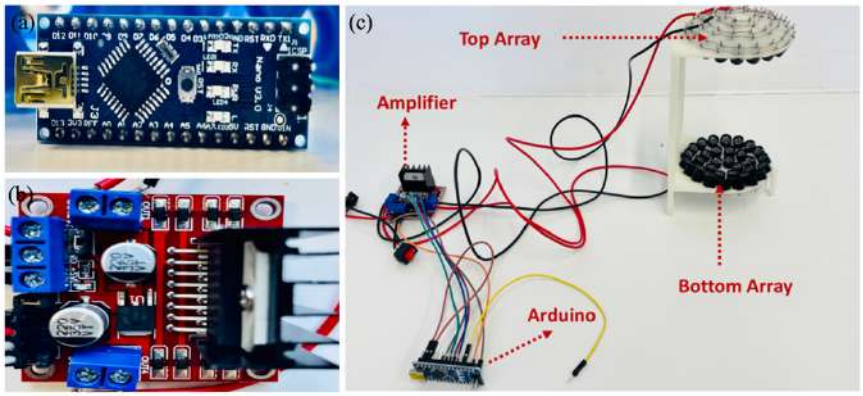

Figure 2.3 Components of the acoustic levitator. (a) Arduino Nano; (b) driver; (c) the setup of the acoustic levitator.

2.6 Suspension of Droplets in the Levitator

A micropipette with the range of 0.5 – 10 μL was used to fill 2 – 6 μL of sample solutions (Figure 2.4). The tip was well dried and cleaned to avoid the electrostatic force. Then, the liquid was injected into the air on the axis of top and bottom arrays. Droplets could be moved up or down by connecting the jumper with one side attached to ground of the Arduino to D3 or D2.

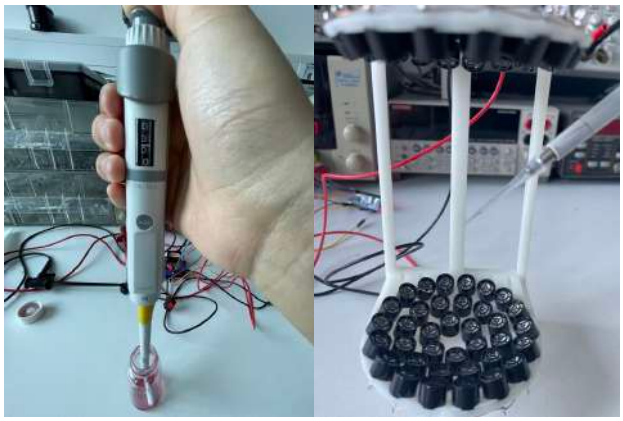

Figure 2.4 Demonstration of suspension process.

2.7 Characterization in POM

Since the assembled products possess liquid crystal properties, polarized optical microscopy (POM) is quite helpful because it is widely used to study transparent optically anisotropic materials. The optical microscopy relies on the refraction of light when light passes through the media and light bends. The sample is placed between two prisms and light bends when it passes through the lens, which helps to focus on the sample. The optical microscopy is equipped with a polarizer which is placed on the way of the light path somewhere before the sample. Also, an analyzer, the second polarizer, is placed in the optical pathway between the

objective rear aperture and the observation tubes or camera port. If the sample is birefringent, in another word, doubly-refracting, it will interact with plane-polarized light and generate two individual wave components polarized in perpendicular planes, thus producing image contrast.

The use of polarized optical microscopy allows determining the nature of the liquid-crystal phases based on the birefringent textures. In addition, the thickness of the materials can be estimated from the birefringent color, as shown in Michel-Lévy color chart.

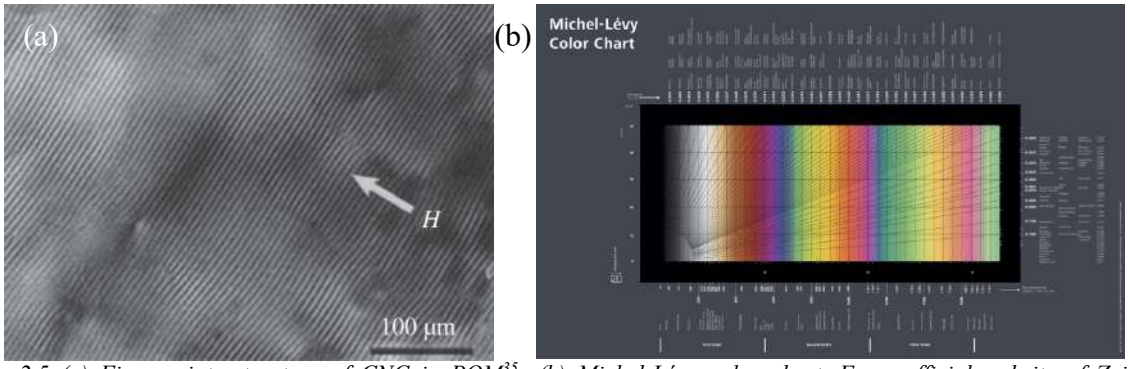

Figure 2.5 (a) Fingerprints structure of CNC in POM[35]; (b) Michel-Lévy color chart. From official website of Zeiss Microscopy.

2.8 Characterization in SEM and Sample Preparation

Electron microscopy technique is indispensable for obtaining high-resolution images of ordered structures consisting of anisotropic NPs. It can help us gain insights into morphology, topographic information, shape, and size both of collective sample and individual particles. There are two main types of electron microscopies: transmission electron microscopy (TEM) and scanning electron microscopy (SEM). In TEM, electron beams transmit through thin specimen to obtain the statistical description of NPs on a local scale. The 2D projection images enable us to explore the interior structure of the sample (especially for imogolite nanotubes) and determine the dimensions of "rod-like" NPs (diameter and length). In the context of SEM technique, the information is from the secondary electrons from the surface generated by the electron beams scanning the surface and interacting with the sample. SEM is powerful to obtain the 3D information of the shape of the assembled products and the interior structures.[8]

CNC bead was at first tested for the tolerance of 50 °C corresponding to the temperature of melting epoxy resin. Then the sample was mounted on the substrate using melting epoxy resin. After the solidification of the resin, the sample was sectioned by ultramicrotome (Leica ARTOS 3D) at Institute for Integrative Biology of the Cell (I2BC, Gif-sur-Yvette, France) until the surface was flat. To avoid the charge effect during the measurement, the resin around the bead was removed as much as possible in ultramicrotome and retrieved from the substrate using blades. Scanning electronic microscopy (SEM) characterization for the cross-sectional surface of the bead was performed at the Laboratoire de Physique des Solides (LPS, Orsay, France) with a Zeiss Supra55VP and an acceleration voltage of 5 keV.

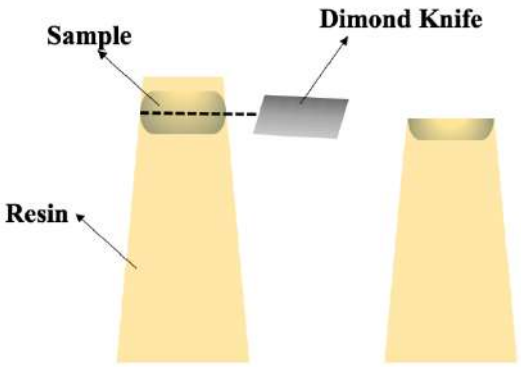

Figure 2.6 Demonstration of sample cutting process.

2.9 Characterization in X-ray Scattering

Small-angle and wide-angle X-ray scattering (SAXS/WAXS) are powerful tools for unravelling various 2D and 3D bulk superstructures. They can be used to identify the symmetry, shape, orientations of the nanoparticles, interspace between particles, and how these nanoparticles reside in the assembled sample. The X-rays beam interacts with the sample. The elastic part of the scattering (i.e., without loss of energy) is collected by a two-dimensional area detector placed behind the sample at a given position. The scattering vector modulus Q is deduced from radial integration of the 2D pattern, where $q = 4\pi\sin(\theta)/\lambda$ (λ is the wavelength of X-rays, θ is scattering angle).[36] Depending on the wavelength, the Q-range can be adjusted to probe large (SAXS) to low (WAXS) distances. The probe length is defined as $D = 2\pi/q$.

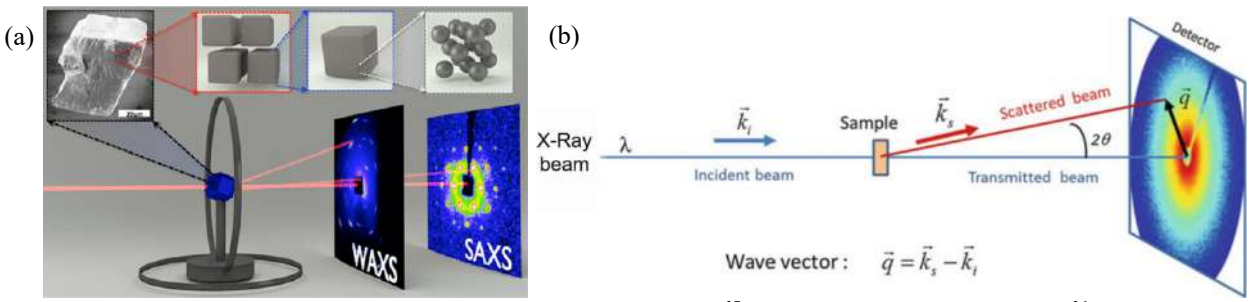

Figure 2.7 (a) Experimental setup of WAXS and SAXS[37]; (b) Optical components of SAXS.[36]

During the measurement, samples were fixed on the conductive sticker and clamped in the sample stage. A pre-scan was applied to find the position of the sample followed by the measurement.

3 Results and Discussion

3.1 Voltage effect on the shape of the droplet

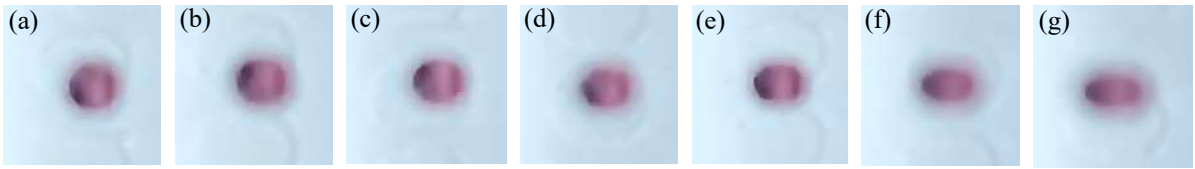

Figure 3.1 The shape of the same droplet stained with Au NPs under the voltage of (a) 6 V; (b) 7 V; (c) 8 V; (d) 9 V; (e) 10 V; (f) 11 V; (g) 12 V.

A droplet stained with Au NPs was levitated at nominal voltage 12 V. Then the voltage was decreased slowly until the droplets fell. The voltage range to suspend a droplet stably as soon as the droplet is injected is from 6 V to 12 V (Figure 3.1). When the voltage ranges from 9 V to 12 V, the droplet with volume of 3 μL can be suspended stably until it is fully dried. When the voltage was increased from 6 V with a progressive increment of 1 V, a shape transition of the droplet could be observed. At 6 V, the droplet appears to be spherical while at 12 V, it looks like a flat "pancake". Between 6 V and 12 V, the transitional shape is elliptical. This phenomenon can be explained by the principle of the acoustic levitator as schematically represented in Figure 3.2.

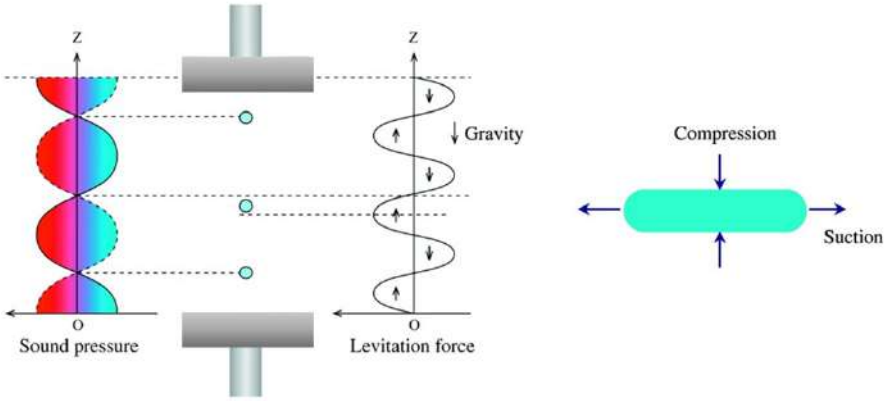

Figure 3.2 Illustration of principles accounting for the shape of the droplet at different voltages. Adapted from Ref 38.

For a solid material, a force is generated by the acoustic levitator to balance the gravity, thus it can be levitated. However, for the levitation of a liquid droplet, the goal is more than balancing gravity. Instead, a force balance at the droplet surface should be achieved. The acoustic radiation pressure due to the standing wave on the droplet is not uniform. The pressure is usually positive at the polar area (also indicated as compression) while negative (known as suction) at the equator. When the droplet is suspended, it will adjust its surface curvature to adapt the radiation pressure determined by the voltage in this case.[38] (Figure 3.2)

3.2 Cellulose Nanocrystals (CNCs)

3.2.1 Comparison between samples dried on the substrate and in the acoustic levitator

The exploration started by CNCs with aspect ratio around 10 which is between those of Au NRs (around 3) and DWINTs (usually more than 50). The same volume of aqueous dispersions of CNCs was dried in the acoustic levitator and on the plastic substrate, respectively. Combining two images characterized from the top and the side in Figure 3.3, we can observe

a “red blood cell” shape with a thin film in the middle, which exhibits birefringence indicating the liquid crystal phase. The possible explanation for this shape is the nonuniform shell thickness during the evaporation process. The sample suffers dual front buckling at both poles and a cavity ingression during the evaporation.[39] The detailed structure of this product will be discussed in the following parts.

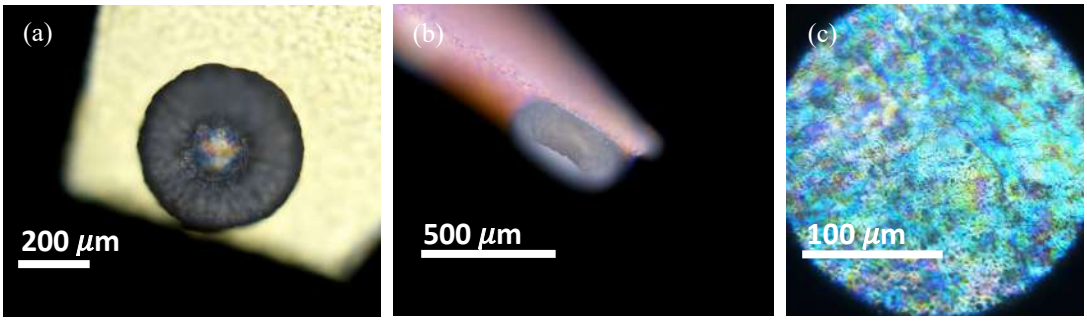

Figure 3.3 3 μL aqueous dispersions of CNCs with concentration of 6 g L^{-1} characterized in POM using bright field mode: (a) (b) dried in the acoustic levitator, viewing from top and side, respectively; (c) dried on the plastic substrate.

By contrast, the product dried from a sessile droplet on the substrate is in the form of thin film and appears to be colorful and birefringent. It is due to the nonuniform thickness of the thin film using EISA method on the substrate. This affects the helix spacing of the chiral nematic structure, which orientates light to different directions, thus various colors can be observed.

3.2.2 Concentration effect on the shape and size

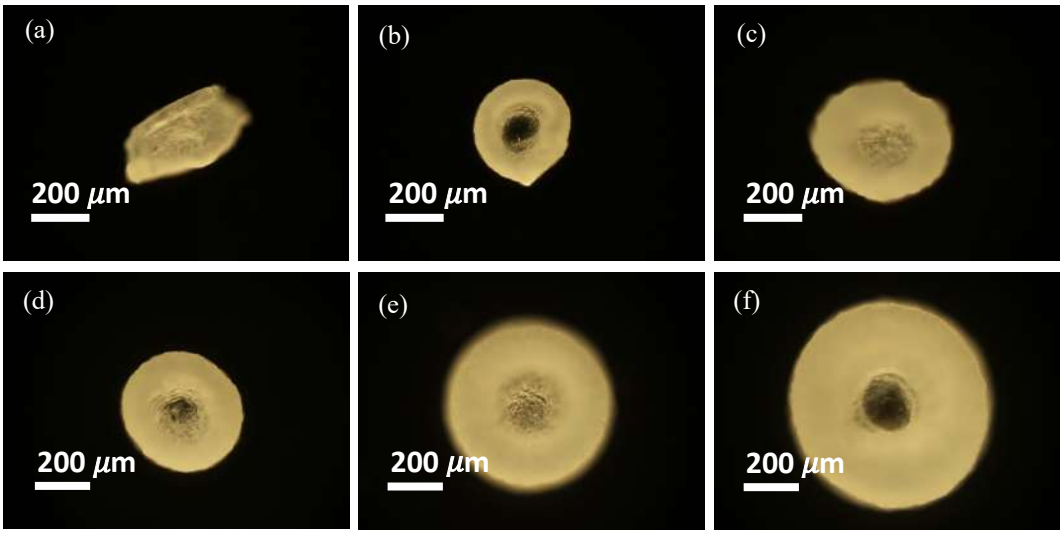

Figure 3.4 3 μL aqueous dispersions of CNCs with different concentrations dried in the acoustic levitator characterized in POM using reflection mode (a) 1 g L^{-1}; (b) 2 g L^{-1}; (c) 6 g L^{-1}; (d) 10 g L^{-1}; (e) 16 g L^{-1}; (f) 32 g L^{-1}.

Further research was conducted to study the effect of concentration on the shape of dried products. A series of concentrations: 1 g L^{-1}; 2 g L^{-1}; 6 g L^{-1}; 10 g L^{-1}; 16 g L^{-1}; 32 g L^{-1} were selected. If the volume fraction ($\phi = c/\rho$, where c is the solid concentration of CNCs and ρ is the density of a CNC, in this case, ~ 1.6 g cm^{-3}) exceeds 6%, gelation occurs, that prevents the formation of a liquid crystal phase. 32 g L^{-1} corresponds to a volume fraction of 2%, i.e., far from the critical concentration of gelation. Though, as the solvent evaporates, the concentration will increase. From Figure 3.3, we know that the final product is in the liquid crystal state. Besides, concentration has an insignificant influence on the shape of dried samples that maintains as a “red blood cell” with a thin film in the middle (Figure 3.4). Then the diameters of dried products were determined to study the relationship between the concentration and the

size. As shown in Figure 3.5, the diameter is proportional to the concentration before 25 g L^{-1}, and afterwards, a plateau can be observed, indicating small changes in the diameter and increase in the thickness as the number of nanotubes and total mass of the droplet increase. Possible reason could be the curvature induced by the force balance on the droplet, which needs to be further investigated.

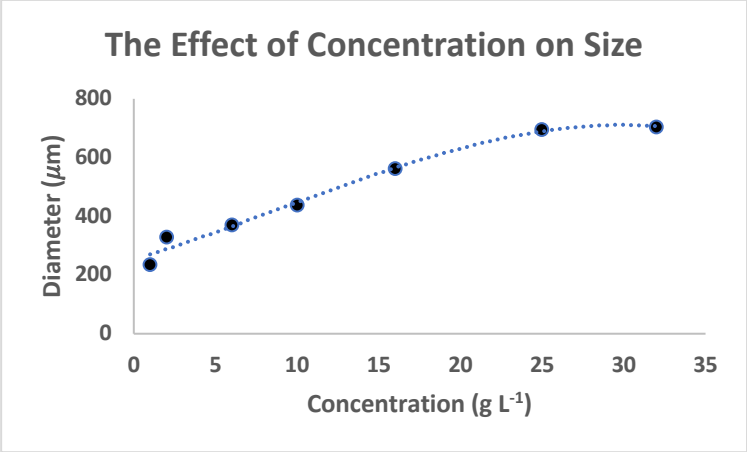

Figure 3.5 The relationship between the concentration of CNCs and the size of the product.

3.2.3 Volume effect on the shape

Different amounts of aqueous dispersion of CNCs were also applied to investigate the effect on the shape. To acquire extremely small volume, fragmentation was carried out by adjusting the voltage to obtain tiny droplets. It's worth here to mention the concept of tactoids. Tactoids are liquid crystalline microdroplets originating from isotropic dispersions and transform into anisotropic phase. When tactoids bear a confinement (i.e., spherical confinement by microfluidic method), several tactoids will coexist in the same microdroplet and merge together. To better adapt to the interface of water/ oil interface, chiral nematic bands will bent and result in the concentric multi-shell structure as shown in Figure 3.6 . [40] Also, a typical Maltese cross will appear due to this configuration.

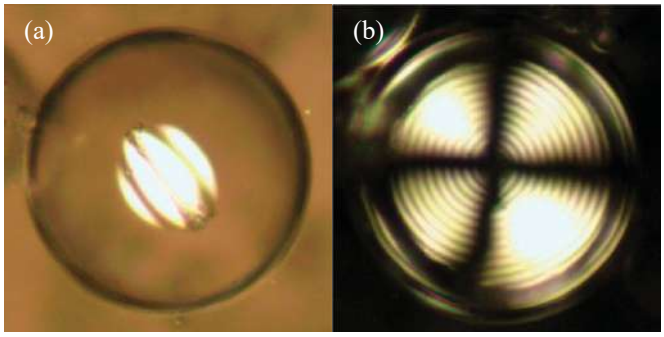

Figure 3.6 Images characterized in POM: (a) tactoids; (b) integrated tactoids. Reprinted from Ref 40.

In Figure 3.7(a), from the background, many tiny dots with Maltese cross can be observed, which is similar to what we get in 2D confinement in liquid. We can also see a bigger droplet dried with topological defects formed when tactoids coalesce. This indicates that the levitated drops provide dispersions with a confined environment. However, only when the volume is small enough, Maltese cross can be observed. When we increase the volume to 3 μL and 6 μL, we can only see the "red blood cell" shape with birefringent middle part. Due to the thickness of peripheral part and the limitation of POM, it's difficult to probe into the inner structure of

the sample. More advanced characterization techniques such as electron microscopy should be applied.

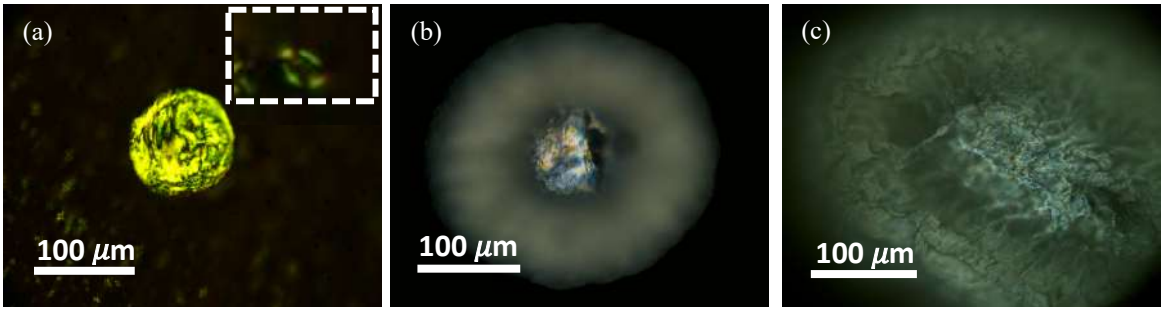

Figure 3.7 2 g L^{-1} aqueous dispersions of CNCs with different volume dried in the acoustic levitator characterized in POM using bright field mode: (a) ~ 0.14 μL with a zoom-in background; (b) 3 μL; (c) 6 μL.

3.2.4 Inner structure and organization

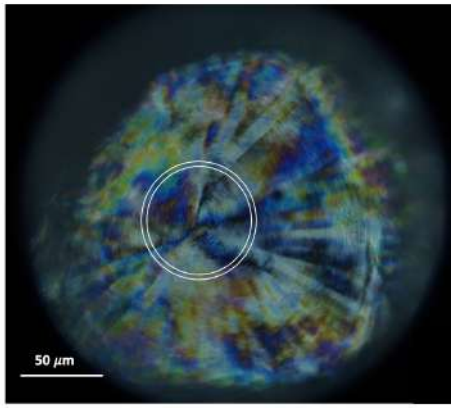

Figure 3.8 3 μL aqueous dispersions of CNCs with concentration of 32 g L^{-1} dried in the acoustic levitator characterized in POM using bright filed mode viewing from the top.

We have not explored the structure and organization of the sample in detail, especially the interesting inner part. As mentioned before, there is a birefringent thin film in the middle of the material. This part of the sample dried from 3 μL aqueous dispersions CNCs with concentration of 32 g L^{-1} was further characterized in POM with higher magnification. The thin film exhibits different colors resulting from different thickness according to Michel-Lévy chart (Figure 2.5). Moreover, topological defects are observed radiating from the center to the edge. If we have a close look at the organization, we can see concentric multi-shell rings as in the case of 2D confinement using microfluidic method. This can be explained by the acoustic levitator that generates acoustic field exerting pressure on the upper and lower parts of the sample. It confines the sample in one direction as the width of the capillary in the microfluidic method, thus it is like a 2D confinement.

To study the "rings" and the inner structure of the thicker part, the sample was cut from the side until we got a flat surface. Then, SEM characterization was applied. When it was examined at lower magnification, a rather smooth surface could be observed. Three spots at different locations of the sample were selected to study fine structure and organization can compared to see the differences. From Figure 3.9(b)-(d), layered structure can be seen across the sample, which is typical chiral nematic microstructures. We cannot observe any significant change in structure between the core and the peripheric parts. The length of the pitch, p, (Figure 1.4(c))

is measured at different spots. Both at the central and the outer parts, the pitch is around 1 µm, which is close to that in the confined droplets.[41]

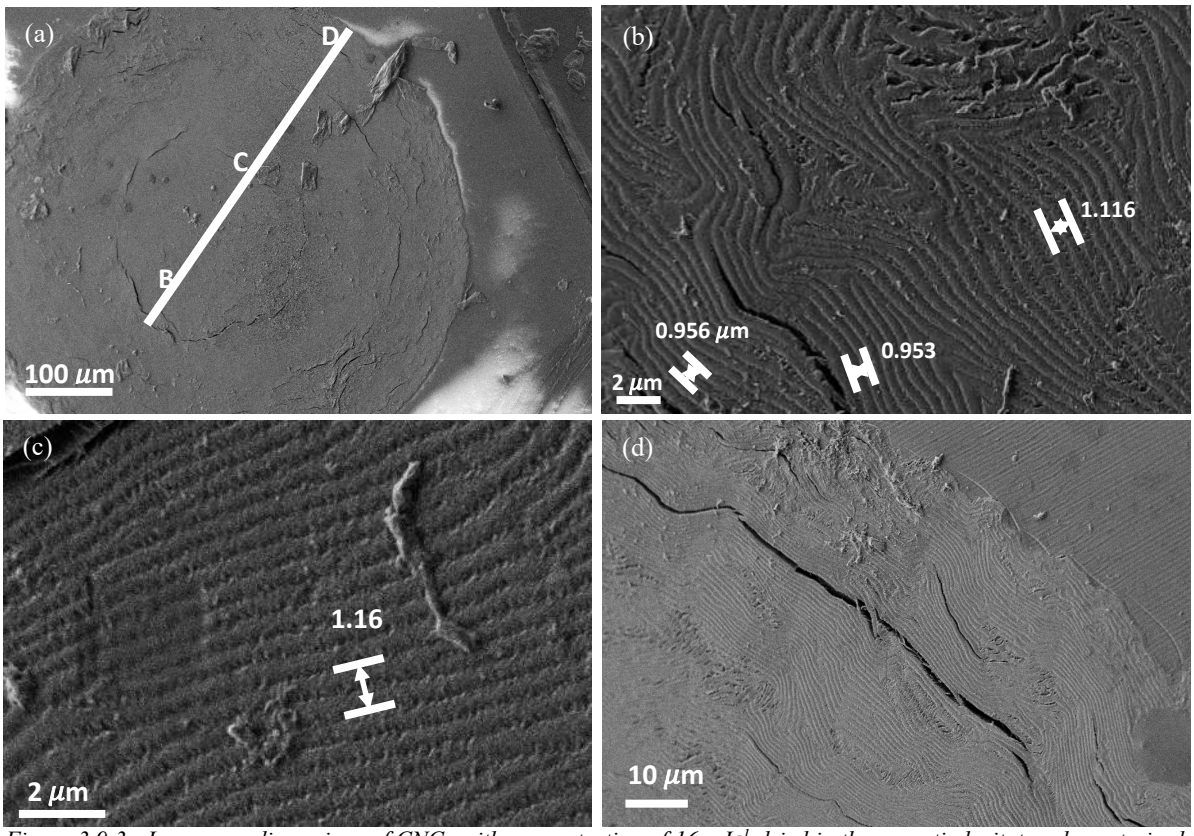

Figure 3.9 3 µL aqueous dispersions of CNCs with concentration of 16 g L^{-1} dried in the acoustic levitator characterized in SEM. (a) cross-sectional overview of the sample; (b) zoom-in image of point B; (c) zoom-in image of point C; (d) zoom-in image of point D.

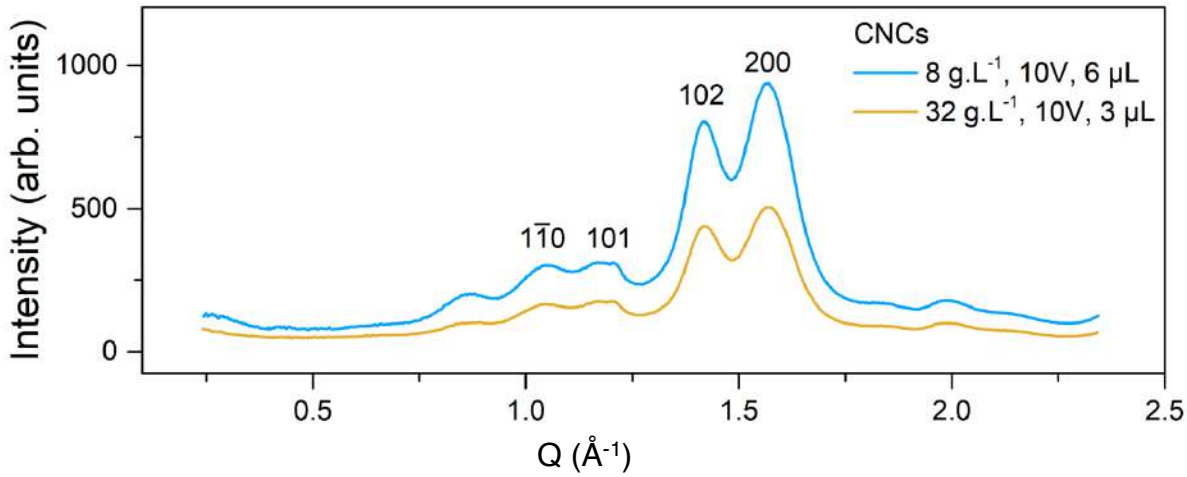

Figure 3.10 WAXS results of dried CNCs using acoustic levitation.

The thin film and the thick side part of the "red blood cell" were examined by X-ray. In both cases, regardless of the number of nanocrystals contained in the sample, similar peaks corresponding to the specific signature of cellulose can be observed. WAXS provides information about crystallinity but limited information about the organization.

3.3 Imogolite Nanotubes (INTs)

3.3.1 Comparison between samples dried on the substrate and in the acoustic levitator

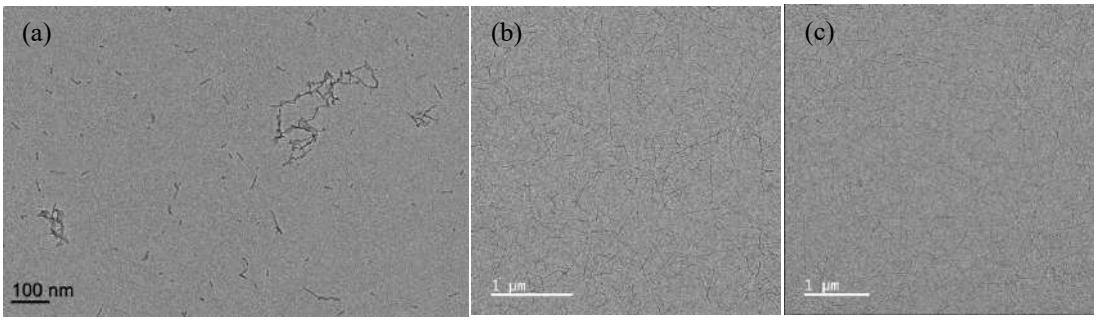

Figure 3.11 TEM images of three batches of imogolite nanotubes with different aspect ratio: (a) batch 1: 4.2 (b) batch 2: 59 (c) batch 3: 357.

Three batches of imogolite nanotubes with different aspect ratio were studied. Direct evaluation of diameters and lengths is obtained by using TEM observations. For all batches, the average diameter of double-wall nanotubes is 4.3±0.3 nm, while the lengths are 18 nm, 255 nm, and 1535 nm respectively. As shown in Figure 3.11, for batch 1 with smallest aspect ratio, nanotubes are very short and tend to merge. In contrast, for batch 3 with largest aspect ratio by extension of dialysis time, nanotubes are mostly very long and dispersed. The length of batch 2 is intermediate, rather long nanotubes can be observed along with shorter ones.

Then, the same volume of batch 2 with concentration of 2.5 g L^{-1} was dried in the acoustic levitator and on the plastic substrate. Similar to the case of CNCs, the sample dried using levitation was characterized in POM from the top and the side. The shape is like a "pancake" with a concave on one side. Compared with CNCs, the sample is thicker, but birefringent edge still can be observed. This can be possibly explained by the phase transition diagram in Figure 1.5(c). As the solvent evaporates, the concentration of nanotubes increases and before the sample is fully dried, it is frozen in the gel state. Due to the characterization limitation of POM, other techniques such as electron microscopy need to be applied. In terms of the dispersion dried on the substrate, it is in the form of a birefringent thin film with randomly oriented nanotubes.

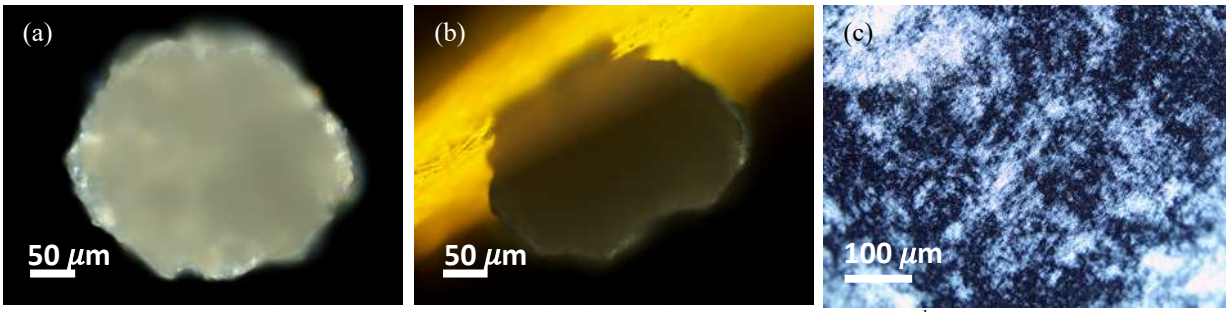

Figure 3.12 3 μL aqueous dispersions of Ge-DWINTs (batch 2) with concentration of 2.5 g L^{-1} characterized in POM using bright field mode: (a) (b) dried in the acoustic levitator, top and side view, respectively; (c) dried on the plastic substrate.

3.3.2 Effect of aspect ratio on the shape

Subsequently, three batches with the same concentration were self-assembled in the acoustic levitator and characterized in POM. The batch with aspect ratio of 357 is in the shape of a bubble with air inside while other two batches possess irregular shapes like thin films packed together. It's worth mentioning that during the injection of liquid into the acoustic levitator, we

can inject air into the droplet easily because of the relatively high viscosity. As the evaporation proceeds, these bubbles either maintain the shape or collapse.

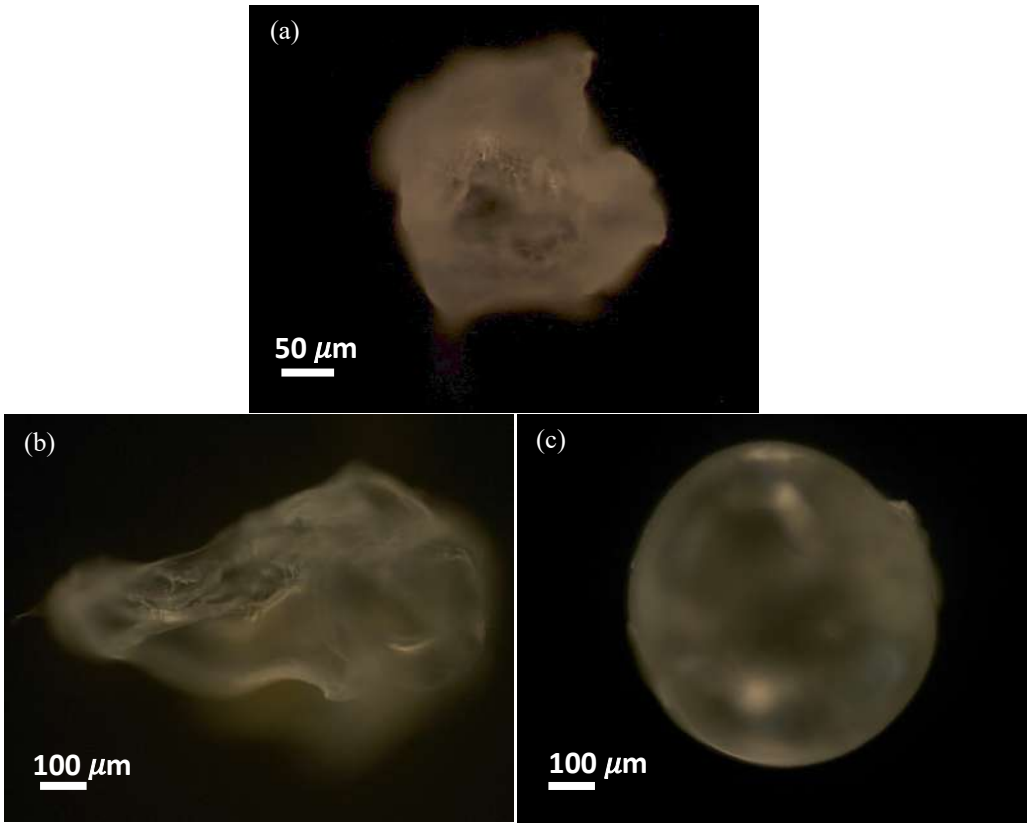

Figure 3.13 3 μL aqueous dispersions of Ge-DWINTs with concentration of 2.5 g L^{-1} characterized in POM using reflection mode: (a)-(c) corresponds to batch 1 to 3 in sequence.

In these cases, the "bubbles" of batch 1 and 2 collapse while it maintains in batch 3. In this scenario, long nanotubes in batch 3 may act as the backbone to resist the migration and rotation during the evaporation process as shown in Figure 3.14.

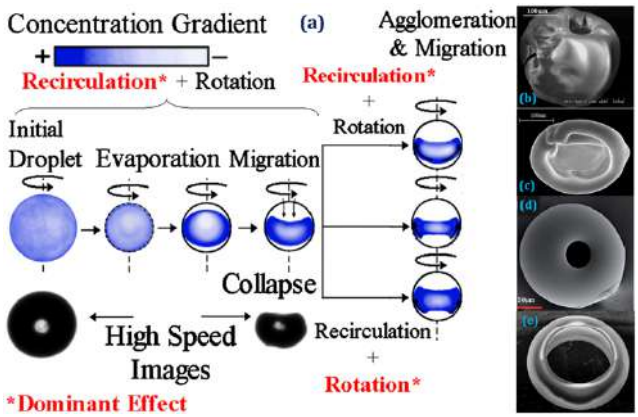

Figure 3.14 Mechanisms responsible for the final structure of droplets levitated in the acoustic levitator. Reprinted from Ref 39.

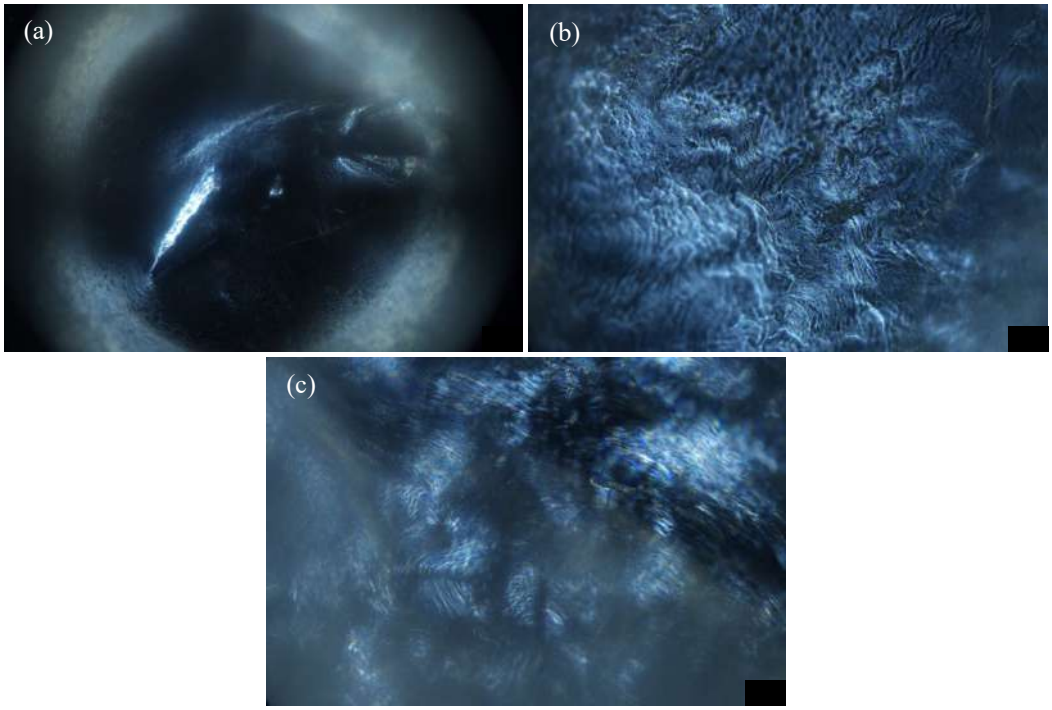

Figure 3.15 3 µL aqueous dispersions of Ge-DWINTs (batch 2) with different concentrations dried in the acoustic levitator characterized in POM using bright field mode: (a) 2.5 g L^{-1}; (b) 5 g L^{-1}; (c) 7.5 g L^{-1}.

Because of the promising hollow structure which can be used as the template to load other materials, batch 2 was further studied by setting a series of concentration. In all cases, the shape of the dried sample in the acoustic levitator is like a "bubble". After the measurement in POM, the sample was crushed, and it turned out to be thin films. The hollow structure can be further confirmed by cutting the sample. Moreover, in POM, the texture of dried suspensions is like hexagonal columnar liquid crystal phase of imogolite nanotubes in aqueous dispersions. This will be further investigated by X-ray scattering techniques.

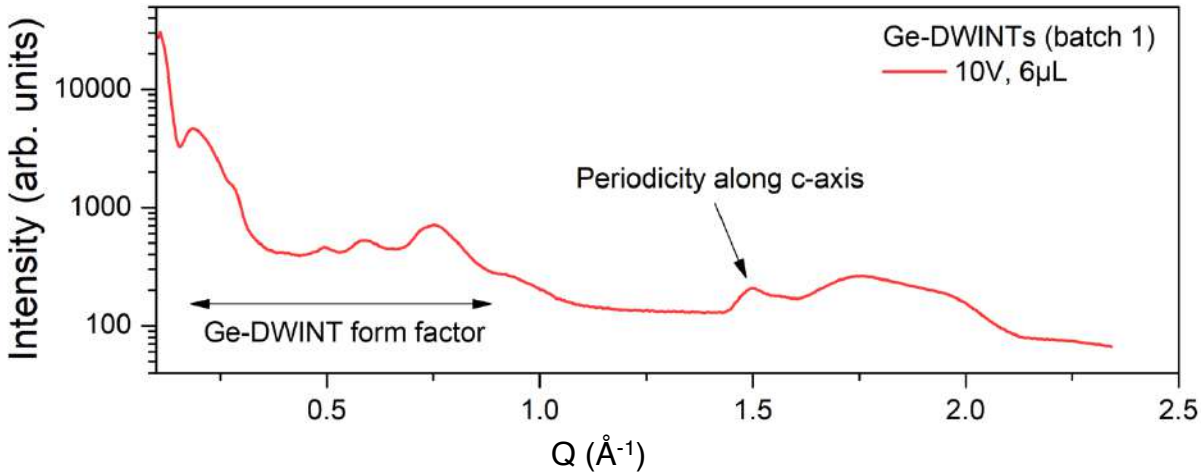

Figure 3.16 WAXS results of dried Ge-DWINTs using acoustic levitation.

In WAXS, we observe the characteristic modulations, an interference of signals from the inner and the outer nanotubes, arising from the form factor of double-walled nanotubes. Another oscillation peak marked on the graph corresponds to the periodicity along c-axis. The combination of these depicts 1D nanotube shape.

The results of WAXS measurements in the lab give us little information on the distance between nanotubes. To acquire this, it is necessary to go to synchrotron to achieve smaller Q value.

3.4 Gold Nanorods (Au NRs)

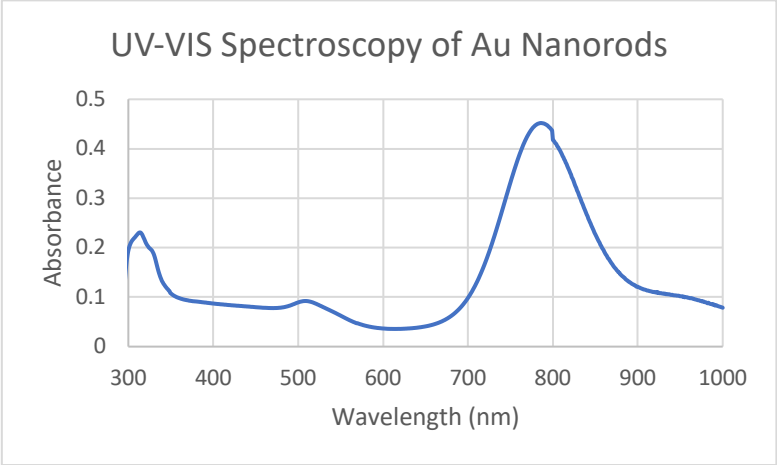

Figure 3.17 UV-vis spectrum of Au NRs.

Scarabelli et. al. proposed an easy method to determine concentration of metallic gold using UV-vis spectrometer. It was found that the extinction cross section (equivalent to absorbance) at 400 nm is identical for all geometries. This is due to the main contribution of absorbance from interband transitions in metallic gold. When the absorbance is 0.6, the corresponding concentration of metallic Au is 0.25 mmol L^{-1}. By doing the calculation, we obtained the concentration of Au as 218 mmol L^{-1}.

3.4.1 Mixture of CNCs and Au NRs

When we tried to suspend the droplet containing Au NRs, we found it difficult to levitate for a long time. This can be explained by the high density of Au which makes it easy to drop and the weak interactions between Au NRs compared with other two materials. Then, aqueous dispersions of Au NRs and CNCs were mixed with different ratio and characterized in POM. Contrary to our expectations, though CNCs and Au NRs have very different aspect ratio, no phase separation was observed in all three cases as shown in Figure 3.18. The shape of the "red blood cell" with a birefringent thin film is maintained and Au NRs are distributed everywhere in the sample due to the uniform color. Here, CNCs act as backbones and support Au NRs.

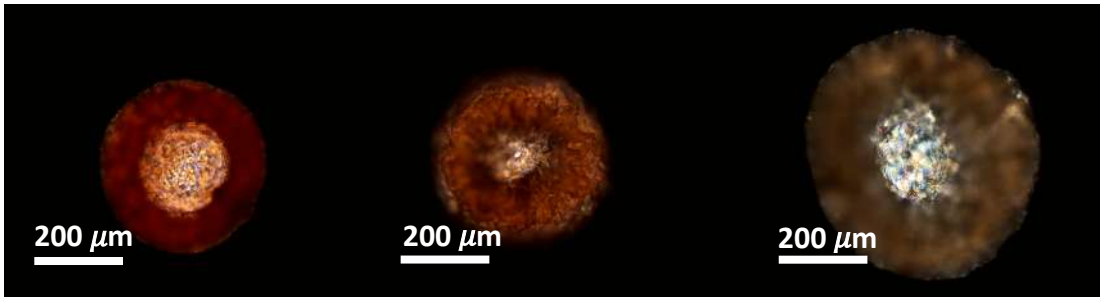

Figure 3.18 Mixture of Au NRs and aqueous dispersions of CNCs with different concentrations of the same volume (3 μL) self-assembled in the acoustic levitator and characterized in POM using bright field mode:(a) 0.352 g L^{-1} Au NRs, 5 g L^{-1} CNCs; (b) 0.352 g L^{-1} Au NRs, 8 g L^{-1} CNCs; (c) 0.352 g L^{-1} Au NRs, 16 g L^{-1} CNCs.

We further characterized the mixture with 0.352 g L^{-1} Au NRs and 5 g L^{-1} CNCs in POM at higher magnification. We can still observe typical "fingerprints" structure with birefringence. However, unlike in the case of pure CNCs with complete concentric rings, only small domains of chiral nematic structure exist in the mixture and these domains distribute irregularly. How Au NRs are distributed in CNCs need to be further investigated by cutting the sample and characterization in SEM.

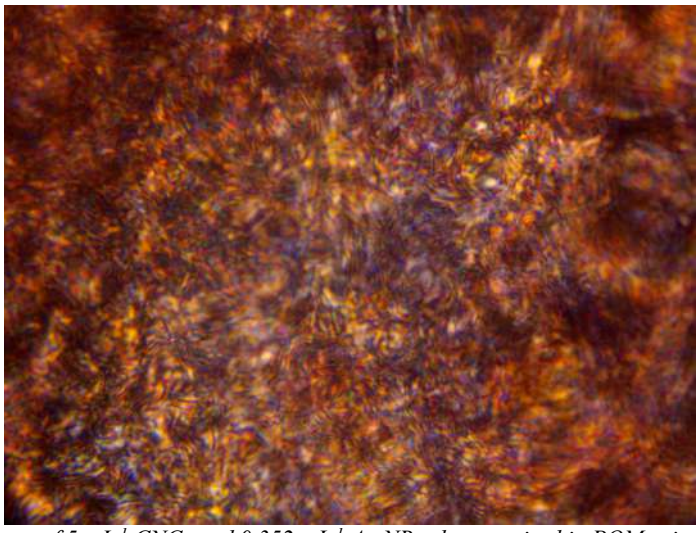

Figure 3.19 A mixture of 5 g L^{-1} CNCs and 0.352 g L^{-1} Au NRs characterized in POM using bright field mode.

4 Conclusion and Perspectives

This work aims to mimic nature by self-assemble anisotropic nano building blocks in confinement in order to generate ordered nanostructures. Acoustic levitation helps to solve the problem of heterogeneous distribution of nanoparticles in evaporation induced self-assembly. The self-assembly is confined by the acoustic standing wave field. The volume of the droplet can be tuned, and the dried sample can be retrieved easily because of avoiding using the substrate. Three "rod-like" materials with different aspect ratios: gold nanoparticles, cellulose nanocrystals, and imogolite nanotubes were synthesized and used to study the effect of aspect ratio on the self-assembly. Compared with the dispersions dried on the substrate, the samples dried in the acoustic levitator show different shapes and organizations for three materials. Concentration and volume effect on the shape and organization were also studied.

By far, we have not figured out a feasible solution to self-assemble Au NRs in the acoustic levitator. Different solvents may strengthen the interactions between Au NRs and using appropriate amount of solution maybe the keys to the self-assembly. These should be further investigated. Also, it's challenging to using X-scattering techniques to see the organization, and to study the interactions between nano particles because of the extreme small size of final products and low contrast with the background, which make it difficult to be detected. In addition, we should take advantage of the acoustic levitator to study EISA in-situ. The self-assembly can be settled in a chamber with the humidity controller to control the evaporation rate while a camera and synchrotron-based X-scattering techniques can be incorporated to study self-assembly in real-time. This simple device is robust for decode the complicate EISA.

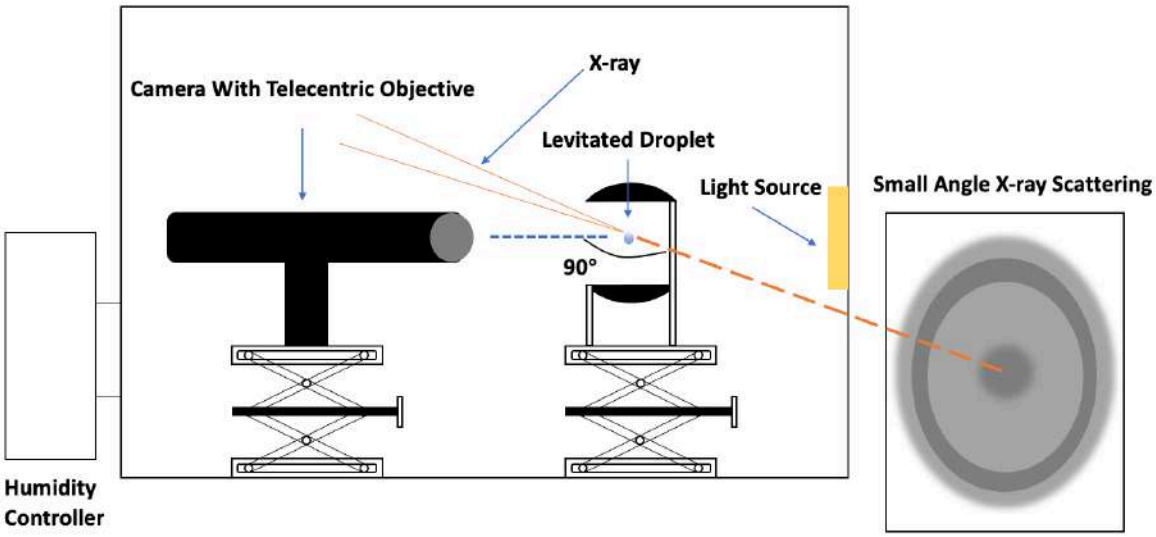

Figure 4.1 The demonstration of the setup to do the in-situ measurement and to study EISA.

References

(1) Weaver James, C.; Milliron Garrett, W.; Miserez, A.; Evans-Lutterodt, K.; Herrera, S.; Gallana, I.; Mershon William, J.; Swanson, B.; Zavattieri, P.; DiMasi, E.; Kisailus, D. The Stomatopod Dactyl Club: A Formidable Damage-Tolerant Biological Hammer. *Science* **2012**, *336* (6086), 1275–1280. https://doi.org/10.1126/science.1218764.

(2) Grason, G. M. Perspective: Geometrically Frustrated Assemblies. *J. Chem. Phys.* **2016**, *145* (11), 110901. https://doi.org/10.1063/1.4962629.

(3) Hamon, C.; Liz-Marzán, L. M. Hierarchical Assembly of Plasmonic Nanoparticles. *Chem. – Eur. J.* **2015**, *21* (28), 9956–9963. https://doi.org/10.1002/chem.201500149.

(4) Pablo F. Damasceno; Michael Engel; Sharon C. Glotzer. Predictive Self-Assembly of Polyhedra into Complex Structures. *Science* **2012**, *337* (6093), 453–457. https://doi.org/doi:10.1126/science.1220869.

(5) Ming, T.; Kou, X.; Chen, H.; Wang, T.; Tam, H.-L.; Cheah, K.-W.; Chen, J.-Y.; Wang, J. Ordered Gold Nanostructure Assemblies Formed By Droplet Evaporation. *Angew. Chem. Int. Ed.* **2008**, *47* (50), 9685–9690. https://doi.org/10.1002/anie.200803642.

(6) Wang, D.; Hermes, M.; Kotni, R.; Wu, Y.; Tasios, N.; Liu, Y.; De Nijs, B.; Van Der Wee, E. B.; Murray, C. B.; Dijkstra, M. Interplay between Spherical Confinement and Particle Shape on the Self-Assembly of Rounded Cubes. *Nat. Commun.* **2018**, *9* (1), 1–10.

(7) Zhu, P.; Kong, T.; Zhou, C.; Lei, L.; Wang, L. Engineering Microstructure with Evaporation-Induced Self-Assembly of Microdroplets. *Small Methods* **2018**, *2* (6), 1800017. https://doi.org/10.1002/smtd.201800017.

(8) Deng, K.; Luo, Z.; Tan, L.; Quan, Z. Self-Assembly of Anisotropic Nanoparticles into Functional Superstructures. *Chem. Soc. Rev.* **2020**, *49* (16), 6002–6038.

(9) Erbil, H. Y. Control of Stain Geometry by Drop Evaporation of Surfactant Containing Dispersions. *Adv Colloid Interface Sci* **2015**, *222*, 275–290. https://doi.org/10.1016/j.cis.2014.08.004.

(10) Deegan, R. D.; Bakajin, O.; Dupont, T. F.; Huber, G.; Nagel, S. R.; Witten, T. A. Capillary Flow as the Cause of Ring Stains from Dried Liquid Drops. *Nature* **1997**, *389* (6653), 827–829.

(11) Deegan, R. D.; Bakajin, O.; Dupont, T. F.; Huber, G.; Nagel, S. R.; Witten, T. A. Contact Line Deposits in an Evaporating Drop. *Phys. Rev. E* **2000**, *62* (1), 756.

(12) Hu, H.; Larson, R. G. Marangoni Effect Reverses Coffee-Ring Depositions. *J. Phys. Chem. B* **2006**, *110* (14), 7090–7094.

(13) Huang, Y.; Zhou, J.; Su, B.; Shi, L.; Wang, J.; Chen, S.; Wang, L.; Zi, J.; Song, Y.; Jiang, L. Colloidal Photonic Crystals with Narrow Stopbands Assembled from Low-Adhesive Superhydrophobic Substrates. *J. Am. Chem. Soc.* **2012**, *134* (41), 17053–17058.

(14) Yunker, P. J.; Still, T.; Lohr, M. A.; Yodh, A. G. Suppression of the Coffee-Ring Effect by Shape-Dependent Capillary Interactions. *Nature* **2011**, *476* (7360), 308–311.

(15) Li, Y.; Yang, Q.; Li, M.; Song, Y. Rate-Dependent Interface Capture beyond the Coffee-Ring Effect. *Sci. Rep.* **2016**, *6* (1), 24628. https://doi.org/10.1038/srep24628.

(16) Cui, L.; Zhang, J.; Zhang, X.; Huang, L.; Wang, Z.; Li, Y.; Gao, H.; Zhu, S.; Wang, T.; Yang, B. Suppression of the Coffee Ring Effect by Hydrosoluble Polymer Additives. *ACS Appl. Mater. Interfaces* **2012**, *4* (5), 2775–2780. https://doi.org/10.1021/am300423p.

(17) Bai, F.; Wang, D.; Huo, Z.; Chen, W.; Liu, L.; Liang, X.; Chen, C.; Wang, X.; Peng, Q.; Li, Y. A Versatile Bottom-up Assembly Approach to Colloidal Spheres from Nanocrystals. *Angew Chem Int Ed Engl* **2007**, *46* (35), 6650–6653. https://doi.org/10.1002/anie.200701355.

(18) Li, Y.; Jun-Yan Suen, J.; Prince, E.; Larin, E. M.; Klinkova, A.; Thérien-Aubin, H.; Zhu, S.; Yang, B.; Helmy, A. S.; Lavrentovich, O. D.; Kumacheva, E. Colloidal Cholesteric

Liquid Crystal in Spherical Confinement. *Nat. Commun.* **2016**, *7* (1), 12520. https://doi.org/10.1038/ncomms12520.
(19) Omrane, A.; Santesson, S.; Alden, M.; Nilsson, S. Laser Techniques in Acoustically Levitated Micro Droplets. *Lab Chip* **2004**, *4* (4), 287–291. https://doi.org/10.1039/b402440k.
(20) Marzo, A.; Barnes, A.; Drinkwater, B. W. TinyLev: A Multi-Emitter Single-Axis Acoustic Levitator. *Rev. Sci. Instrum.* **2017**, *88* (8), 085105. https://doi.org/10.1063/1.4989995.
(21) Tiffany Abitbol; Emily D. Cranston. Chiral Nematic Self-Assembly of Cellulose Nanocrystals in Suspensions and Solid Films. In *Handbook of Green Materials*; pp 37–56.
(22) Wang, P.-X.; Hamad, W. Y.; MacLachlan, M. J. Structure and Transformation of Tactoids in Cellulose Nanocrystal Suspensions. *Nat. Commun.* **2016**, *7* (1), 11515. https://doi.org/10.1038/ncomms11515.
(23) Schütz, C.; Agthe, M.; Fall, A. B.; Gordeyeva, K.; Guccini, V.; Salajková, M.; Plivelic, T. S.; Lagerwall, J. P. F.; Salazar-Alvarez, G.; Bergström, L. Rod Packing in Chiral Nematic Cellulose Nanocrystal Dispersions Studied by Small-Angle X-Ray Scattering and Laser Diffraction. *Langmuir* **2015**, *31* (23), 6507–6513. https://doi.org/10.1021/acs.langmuir.5b00924.
(24) Yoshinaga, N.; Aomine, S. Imogolite in Some Ando Soils. *Soil Sci. Plant Nutr.* **1962**, *8* (3), 22–29. https://doi.org/10.1080/00380768.1962.10430993.
(25) Guimarães, L.; Enyashin, A. N.; Frenzel, J.; Heine, T.; Duarte, H. A.; Seifert, G. Imogolite Nanotubes: Stability, Electronic, and Mechanical Properties. *ACS Nano* **2007**, *1* (4), 362–368. https://doi.org/10.1021/nn700184k.
(26) Paineau, E.; Rouzière, S.; Monet, G.; Diogo, C. C.; Morfin, I.; Launois, P. Role of Initial Precursors on the Liquid-Crystalline Phase Behavior of Synthetic Aluminogermanate Imogolite Nanotubes. *J. Colloid Interface Sci.* **2020**, *580*, 275–285. https://doi.org/10.1016/j.jcis.2020.07.036.
(27) Paineau, E.; Amara, M. S.; Monet, G.; Peyre, V.; Rouzière, S.; Launois, P. Effect of Ionic Strength on the Bundling of Metal Oxide Imogolite Nanotubes. *J. Phys. Chem. C* **2017**, *121* (39), 21740–21749. https://doi.org/10.1021/acs.jpcc.7b07391.
(28) Amara, M.-S.; Paineau, E.; Bacia-Verloop, M.; Krapf, M.-E. M.; Davidson, P.; Belloni, L.; Levard, C.; Rose, J.; Launois, P.; Thill, A. Single-Step Formation of Micron Long (OH)3Al2O3Ge(OH) Imogolite-like Nanotubes. *Chem. Commun.* **2013**, *49* (96), 11284–11286. https://doi.org/10.1039/C3CC46839A.
(29) Nasr-Esfahani, P.; Ensafi, A. A. 7 - Noble Metals and Nonnoble Metal Oxides Based Electrochemical Sensors. In *Functionalized Nanomaterial-Based Electrochemical Sensors*; Hussain, C. M., Manjunatha, J. G., Eds.; Woodhead Publishing, 2022; pp 115–140.
(30) Achanta, V. G. Surface Waves at Metal-Dielectric Interfaces: Material Science Perspective. *Rev. Phys.* **2020**, *5*, 100041. https://doi.org/10.1016/j.revip.2020.100041.
(31) Louis, C.; Pluchery, O. *Gold Nanoparticles for Physics, Chemistry and Biology*; World Scientific, 2017.
(32) Jana, N. R.; Gearheart, L.; Murphy, C. J. Seed-Mediated Growth Approach for Shape-Controlled Synthesis of Spheroidal and Rod-like Gold Nanoparticles Using a Surfactant Template. *Adv. Mater.* **2001**, *13* (18), 1389–1393. https://doi.org/10.1002/1521-4095(200109)13:18<1389::AID-ADMA1389>3.0.CO;2-F.
(33) Tartaj, P.; del Puerto Morales, M.; Veintemillas-Verdaguer, S.; González-Carreño, T.; Serna, C. J. The Preparation of Magnetic Nanoparticles for Applications in Biomedicine. *J. Phys. Appl. Phys.* **2003**, *36* (13), R182.

(34) Lu, X.; Rycenga, M.; Skrabalak, S. E.; Wiley, B.; Xia, Y. Chemical Synthesis of Novel Plasmonic Nanoparticles. *Annu. Rev. Phys. Chem.* **2009**, *60*, 167–192.
(35) Wang, P.-X.; MacLachlan, M. J. Liquid Crystalline Tactoids: Ordered Structure, Defective Coalescence and Evolution in Confined Geometries. *Philos. Trans. R. Soc. Math. Phys. Eng. Sci.* **2018**, *376* (2112), 20170042. https://doi.org/10.1098/rsta.2017.0042.
(36) Barré, L. *Contribution of Small-Angle X-Ray and Neutron Scattering (SAXS and SANS) to the Characterization of Natural Nanomaterials: Datasheet from · Volume : "X-Ray and Neutron Techniques for Nanomaterials Characterization" in SpringerMaterials (Https://Doi.Org/10.1007/978-3-662-48606-1_12)*; Springer-Verlag Berlin Heidelberg.
(37) Li, R.; Bian, K.; Wang, Y.; Xu, H.; Hollingsworth, J. A.; Hanrath, T.; Fang, J.; Wang, Z. An Obtuse Rhombohedral Superlattice Assembled by Pt Nanocubes. *Nano Lett.* **2015**, *15* (9), 6254–6260. https://doi.org/10.1021/acs.nanolett.5b02879.
(38) Zang, D.; Yu, Y.; Chen, Z.; Li, X.; Wu, H.; Geng, X. Acoustic Levitation of Liquid Drops: Dynamics, Manipulation and Phase Transitions. *Adv. Colloid Interface Sci.* **2017**, *243*, 77–85.
(39) Pandey, K.; Prabhakaran, D.; Basu, S. Review of Transport Processes and Particle Self-Assembly in Acoustically Levitated Nanofluid Droplets. *Phys. Fluids* **2019**, *31* (11), 112102.
(40) Wang, P.-X.; Hamad, W. Y.; MacLachlan, M. J. Polymer and Mesoporous Silica Microspheres with Chiral Nematic Order from Cellulose Nanocrystals. *Angew. Chem.* **2016**, *128* (40), 12648–12652.
(41) Parker, R. M.; Frka-Petesic, B.; Guidetti, G.; Kamita, G.; Consani, G.; Abell, C.; Vignolini, S. Hierarchical Self-Assembly of Cellulose Nanocrystals in a Confined Geometry. *ACS Nano* **2016**, *10* (9), 8443–8449. https://doi.org/10.1021/acsnano.6b03355.